Hybrid CoMoS - polyaniline nanowires catalysts for hydrodesulfurisation applications

Sourav Ghosh[1,#], Laurence Courthéoux[2], Sylvette Brunet[3], Patrick Lacroix-Desmazes[2], Annie Pradel[2], Etienne Girard[1,*], Denis Uzio[1,*]

[1] *IFPEN, Rond-point de l'échangeur de Solaize, BP3, Solaize, France*

[2] *ICGM, Univ. Montpellier, CNRS, ENSCM, Montpellier, France*

[3]*IC2MP,Univ.Poitiers, UMR 7285 CNRS, Poitiers, France*

* Corresponding author email: etienne.girard@ifpen.fr, denis.uzio@ifpen.fr

[#]Current address: Laboratoire de Physique et Chimie des Nano Objets, INSA, Université de Toulouse, 135, Avenue de Rangueil, 31077 Toulouse, France.

Keywords: CoMoS catalyst, nano-hybrid, hydrodesulfurisation, olefins hydrogenation, polyaniline

Highlights:

- Liquid and gas phase sulfidation conditions of MoO_x/PANI hybrids result in different MoS_x phases
- Active CoMoS phase content in the final catalysts deposited through a surface reaction using cobalt acetylacetonate depends on the nature of starting Mo based PANI materials. The formation of mixed sites is favored when Mo and Co sulfidations are simultaneous.
- CoMoS/PANI showed much better catalytic activities than the CoMoS counterpart prepared without PANI
- HDS of 3-methylthiophene is correlated to the $Co/Mo_{edges+corners}$ atomic ratio as well as the HDS / HYD selectivity factor.

Abstract

Catalytic performances of promoted CoMoS catalysts were greatly improved via a synthesis strategy based on the structuration of the active phase using self-assembled PANI (Polyaniline)

nanowires followed by an addition step of cobalt acetylacetonate on oxidic or sulfided Mo-based hybrids. Taking into account the different promotion levels, slabs lengths determined by XPS and TEM, the highest rate constants normalized by mol of $(MoS_2)_{edges+corner}$ in the hydrodesulfurization of 3-methylthiophene were obtained when $Co(acac)_2$ is deposited on a MoS_3/PANI hybrid precursor. The normalized HDS rate constants for the different samples followed the increase in $Co/Mo_{edges+corner}$ atomic ratios whereas an optimum for HDS/HYD selectivity in the same ratio was observed.

1. Introduction

In the recent decades, worldwide regulations of fuels combined with the processing of heavier hydrocarbon resources as well as the increase of the global energy demand have driven the development of evermore active hydrotreatment catalysts. For instance, production of "sulfur free" gasoline (less than 10 ppm since 2009) has received significant attention over the years and still is a hot topic of environmental catalysis [1,2]. Conventional hydrotreatment catalysts are made of nanometer-sized molybdenum or tungsten sulfide slabs supported on oxidic carriers, where the edge sites of the slabs promoted by nickel or cobalt are considered as the active sites [3]. However, these supported catalysts suffer strong limitations when high metal loadings combined with high active phase dispersion are targeted. So far, in order to improve the catalytic performances, many studies have focused on modification of supports by addition of organic [1,3,4-8] and inorganic additives [1,3,4,6,9-11], type of supports [1,3,4,6,12-14], and active phase modifications [1,3,4,6,15-19]. Nowadays, a breakthrough in terms of activity seems difficult to achieve through these strategies and the alternative way could be the development of unsupported bulk sulfide catalysts to drastically increase the active phase content per volume and the performances accordingly [1,20,21].

Typical synthesis of bulk unsupported samples consists in thermal decomposition or (co) precipitation of (oxo)thio salts under various experimental conditions [6,22-27]. However, these approaches are often not suitable to achieve highly efficient catalysts since a large fraction of the metallic sites does not participate to the reaction due to a poor accessibility. Moreover, a nanoscale control of the bimetallic composition is difficult to achieve on bulk catalysts. Hence, in order to prepare an optimized catalyst, the control of the individual slabs properties at the nanoscale is mandatory to maximize the intrinsic activity and as well as the control of their mesostructure for active site accessibility and diffusion purposes. These considerations have

been addressed in previous reports playing on synthesis methods of bulk CoMoS catalysts for FCC gasoline hydrodesulfurisation. Zhang *et al*. have reported that the slab size and stacking of MoS_2 could be tuned under hydrothermal conditions by changing the pH and precursors, which in turn determine the HDS selectivity in of FCC gasoline [28]. In a different report, Li *et. al*. demonstrated that unsupported Co-Mo catalysts prepared using ion-exchange reaction of cobalt carbonate hydroxide as precursor followed by a gas-phase sulfidation, exhibit higher HDS selectivity for both model molecule and full-range FCC gasoline than supported CoMo/γ-Al_2O_3. The improvement was explained in terms of slab length, number of layers and curvature of the slabs [29]. Concerning this last feature, Afanasiev *et al* have shown that inorganic "fullerene-like" structures of MoS_2 (onion-like or hollow MoS_2) are active towards thiophene HDS and the curved and/or broken basal planes are found to exhibit high activity. [30,31].

In order to achieve a high dispersion and accessibility of active phases, template-assisted synthesis has been carried out using soft and hard templates for the synthesis of bulk mesostructured metal sulfide catalysts [4,6,23]. Several organic templates including surfactants (ionic and non-ionic) and polymers (polyethylene glycol, pluronic 123 (P123), polyvinylpyrrolidone (PVP), etc) have been extensively used as soft template for synthesis of high surface area unsupported bulk catalysts [6,23,32-35]. In order to control the physicochemical properties (size, aggregation, and accessibility/orientation), electronic properties of the active sites, synthesis of MoS_2 using a polymer as a template recently appeared as a promising alternative [23]. Similarly, bulk unsupported catalysts were also synthesized using the hard template route [6,36-38]. However, many challenges still exist to improve bulk HDS catalysts features such as an optimum dispersion and accessibility of the edge sites to reactants / products, sintering resistance for deactivation issues, control of the promotion at high metal loading and control of the assembling of individual slabs for mass transfer properties. It can be also noticed that this type of catalysts suffer from a lack of studies compared with supported counterparts.

The present work gets inspired by the design of MoS_2/PANI (Polyaniline) hierarchical nanostructures for lithium-ion batteries wherein, the nanoscale dimension of MoS_2 promotes the kinetics of Li^+ ion storage due to the shortened diffusion paths, while PANI nanowires effectively avoid aggregation of the active nano slabs and ease the transport of electrons and ions [38]. Applied to HDS reaction, the unique arrangement of the MoS_2 slabs at the surface is supposed to favor the exposure of more active edges to reactants. The work presented in this manuscript will therefore focus on the synthesis of bulk promoted (Co)MoS_2 catalysts via

polymerisation induced self-assembly, using polyaniline as a nucleating-growth agent for molybdenum sulfide slabs (Figure 1). In particular, different routes for the formation of the promoted CoMoS phase have been investigated adding Co on MoO_x/PANI oxidic phase or on MoS_x/PANI sulfide one. The characterizations of the solids by scanning and transmission electron microscopy (SEM/TEM), as well as Raman and X-Ray photoelectron (XPS) spectroscopies will be presented and discussed in relation with the catalytic performances in selective HDS.

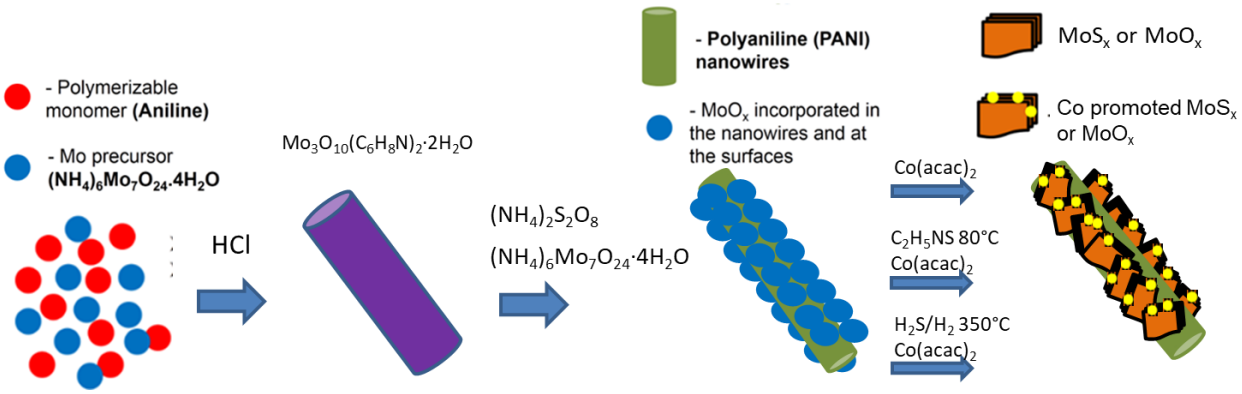

Figure 1 : Schematic representation of the preparation of nanohybrid CoMoS catalysts embedded with polyaniline self-assembled nanowires.

2. Experimental

2.1 Synthesis

-Materials

Aniline, thioacetamide, ammonium heptamolybdate ($(NH_4)_6Mo_7O_{24}\cdot 4H_2O$), cobalt acetylacetonate ($Co(acac)_2\cdot 2xH_2O$) and ammonium persulfate ($(NH_4)_2S_2O_8$) were purchased from Sigma Aldrich. Hydrochloric acid (HCl), methanol, acetone and ethanol were obtained from VWR International. All analytical grade chemicals were used as received until specified. All the reaction were carried out using a doubly distilled water obtained from a Millipore system. γ-Alumina used for dilution was provided by Axens.

- Synthesis of $Mo_3O_{10}(C_6H_8N)_2\cdot 2H_2O$ nanowires

The synthesis of $Mo_3O_{10}(C_6H_8N)_2\cdot 2H_2O$ molecular precursor and the subsequent polymerisation step are adapted from the literature [38]. Typically, 7.44 g (6 mmol) of $(NH_4)_6Mo_7O_{24}\cdot 4H_2O$ (M = 1235.86 g/mol) was dissolved in 120 mL of water. Then 10.02 g

(107.6 mmol) of aniline (M=93.13 g/mol) was added (aniline:Mo = 2.5:1 molar ratio) . Subsequently, 1M HCl aqueous solution was added under vigorously stirring condition at 30°C until a white precipitate appeared (pH=4-5). The reaction mixture was stirred at 50°C for 2 h. The white product of $Mo_3O_{10}(C_6H_8N)_2 \cdot 2H_2O$ nanowires was filtered and washed one time with water and three times with ethanol and dried under vacuum at 50°C for 6 h.

- Synthesis of MoO_x/PANI

0.68 g (1 mmol) of $Mo_3O_{10}(C_6H_8N)_2 \cdot 2H_2O$ (M= 672.17 g/mol), 0.538 g (0.435 mmol) of $(NH_4)_6Mo_7O_{24} \cdot 4H_2O$ and 1.14 g (5 mmol) of $(NH_4)_2S_2O_8$ (M=228.20 g/mol) were added in 80 mL of water, and the pH was adjusted to 2 by adding 5mL of a 1M HCl aqueous solution. After vigorously stirring at 30°C for 6 h, the dark green precipitate of MoO_x/PANI was filtered and washed four times with water and ethanol and dried under vacuum for 6 h at 50°C.

- Sulfidation of MoO_x/PANI

- ***Liquid-phase sulfidation at 80°C***

At first, 3 g of MoO_x/PANI was dispersed in 60 mL of aqueous HCl solution (pH=1) and the solution was heated up to 80°C. Then, 3 g (40 mmol) of thioacetamide (M=75.13 g/mol) (S:Mo~3:1 molar ratio) was added in the reaction mixture and vigorously stirred for 3 h at 80°C. After naturally cooling, the black precipitate was filtered and washed four times with water and ethanol and dried under vacuum for 6 h at 50°C. The MoS_x/PANI powder was stored under an argon filled glove box. The sample was abbreviated as MoS_x/PANI_thioA.

- ***Gas-phase sulfidation at 350°C***

An aliquot of the MoO_x/PANI was sulfided in gas-phase sulfo-reductive conditions (H_2S/H_2 15:85 v/v) at atmospheric pressure. Firstly, MoO_x/PANI powder was transferred in a quartz reactor and heated 2 h at 350°C (heating ramp 5°C min^{-1}) under H_2S/H_2 constant flow (2 $Lh^{-1}g^{-1}$). After the plateau, the reactor was cooled down naturally under the flow of H_2S/H_2 mixture, which was replaced at 50°C by argon during 10 min. Finally, the reactor was evacuated (~1 mbar) and transferred inside an argon filled glove box. The sample was named as MoS_x/PANI_H_2S.

- Cobalt promotion step the molybdenum phases

The promotion step with cobalt acetylacetonate $Co(C_5H_7O_2)_2.2H_2O$ (257.15 g/mol) under reflux conditions was carried out following the procedure developed by Bezverkhyy *et al*. [39] In a typical synthesis, required amount of $Co(C_5H_7O_2)_2.2H_2O$ (Co:Mo=0.4 mol:mol) was dissolved in a minimum amount of degassed methanol and then the catalyst (MoO_x/PANI or MoS_x/PANI) was added and the reaction mixture was refluxed at 30°C for 18 h under Ar atmosphere. After that, methanol was evaporated and the solids were dried under vacuum at 50°C for 6 h. In order to improve the chemical interaction with the MoO_x/PANI surface, we modified this protocol by heating at 65°C for 4 h during $Co(acac)_2$ impregnation, removing the excess of unreacted Co by filtration/washing and finally drying under vacuum for 6 h at 50°C. Table 1 summarizes the different preparations.

Table 1: Abbreviation and synthesis conditions of the different samples.

catalyst	**Synthesis condition**
Unpromoted	
MoO_x/PANI	$Mo_3O_{10}(C_6H_8N)_2 \cdot 2H_2O$, $(NH_4)_2S_2O_8$, $(NH_4)_6Mo_7O_{24} \cdot 4H_2O$, water; pH=2, 30°C, 6 h stir
MoS_x/PANI_thioA	MoO_x/PANI, thioacetamide (Mo:S=1:3 mol/mol), water; 80°C, 3h stir, pH=1
MoS_x/PANI_H_2S	MoO_x/PANI; 15:85 v/v H_2S:H_2, 350°C, 2 h
Promoted	
$CoMoO_x$/PANI_30	MoO_x/PANI, $Co(acac)_2$, methanol; 30°C, 18 h stir (Ar)
$CoMoS_x$/PANI_thioA_30	MoS_x/PANI_thioA, $Co(acac)_2$, methanol; 30°C, 18h stir (Ar)
$CoMoS_x$/PANI_H_2S_30	MoS_x/PANI_H_2S, $Co(acac)_2$, methanol; 30°C, 18 h stir (Ar)
$CoMoO_x$/PANI_65	MoO_x/PANI, $Co(acac)_2$, methanol; 65°C, 4 h stir (Ar) filtration/washing
Ref CoMoS *	MoS_x_H_2S, $Co(acac)_2$, methanol; 30°C, 18 h stir (Ar)

*: details for the synthesis of the Ref CoMoS catalyst are given in the SI

2.2 Characterizations before catalytic tests

Powder X-ray diffraction (XRD), CHNS elemental analysis, X-Ray fluorescence (XRF), Fourier transformed infrared (FTIR) and Raman spectroscopies, SEM, and N_2 physisorption measurements were carried out on the different samples before Co addition. After Co deposition, samples were further characterized by powder XRD, CHNS elemental analysis and XRF. The details of these experiments are available in the SI.

2.3 Catalytic tests

All the catalysts were diluted with high surface area γ-Al_2O_3 (S_{BET} = 265 m^2g^{-1}). The γ-Al_2O_3 extrudates were grinded using a ball mill, the powder was sieved and the fraction below 64 μm was collected for a better mixing with the catalyst. The Al_2O_3 powder was mixed with the catalyst in order to achieve 10 wt% equivalent MoO_3 loading in the final solid (γ-Al_2O_3+catalyst) and the mixture was further ball milled (3 min, 25 Hz). Afterwards, the powder was pelletized and sieved to collect the 0.355-1.25 mm fraction. This fraction was used for the catalytic tests.

HDS test of 3-methylthiophene (3-MT) in presence of 2,3-dimethyl-2-butene (2,3-DM2BN) (model FCC gasoline feedstock: 0.3 wt% 3-MT, 10 wt% 2,3-DM2BN dissolved in n-heptane 89.7 wt%) was carried out in a Flowrence Avantium unit. Each fixed bed reactor was loaded with 0.3 mL of catalyst. The catalyst activation was carried out using DMDS (4 wt%) in n-heptane (96 wt%) at a LHSV of 3 h^{-1} and a total pressure of 15 bar raising the temperature from room temperature to 350°C (2°C/min) with a plateau of 2 h and H_2/HC ratio of 300 NL/L. After this sulfidation step, temperature was decreased from 350°C to 190°C and the catalysts were tested at four different temperatures (190, 200, 210, and 215°C). LHSV was maintained at 6 h^{-1}, total pressure at 15 bar with H_2/HC of 300 NL/L. The reaction mixture was analyzed by gas chromatography using a DB1 column. The relative uncertainty on the measurement of conversions is 5%. Apparent first order rate constant (*k*, h^{-1}) was evaluated using the following expression (2):

$$k_{HDS\ or\ HYD} = \frac{LHSV}{\%\ MoS_2\ edges + corner} * \ln\left(\frac{1}{1 - x_{HDS\ or\ HYD}}\right) \qquad (2)$$

Here, x is the HDS of 3-MT or hydrogenation (HYD) of 2,3-DM2BN. Normalization by $(MoS_2)_{edges+corner}$ loaded in the reactor was made using XPS and TEM results applying the hexagonal geometric model for MoS_2 sulfide slabs [40].

3. Results and discussion

3.1 Characterization of unpromoted samples

Figure 2 shows the SEM images of MoO_x/PANI, MoS_x/PANI_thioA, and MoS_x/PANI_H_2S. Nanowire morphologies with diameters ranging between 100-500 nm and length between 5 to

20 µm are distinguishly observed in the three samples (Figure S1); the morphological data are comparable to the ones reported in the literature [38] showing the good reproducibility of the synthesis. All three samples present a granular aspect corresponding to Mo based particles homogeneously distributed on the surface of the nanowires. Nevertheless, a mode disordered structure can be observed in the case of MoS_x/PANI_H_2S likely due to the partial decomposition of PANI nanorods.

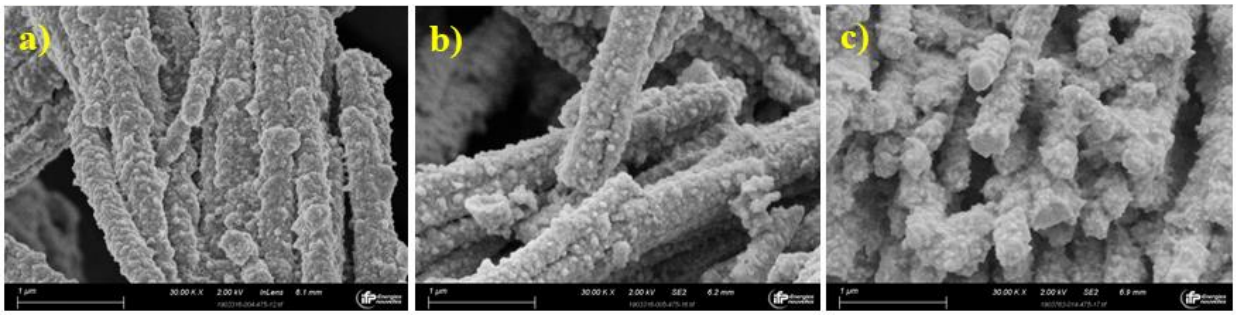

Figure 2. Effect of sulfidation conditions on morphology; SEM images of a) MoO_x/PANI, b) MoS_x/PANI_thioA, and c) MoS_x/PANI_H_2S.

BET surface areas and elemental analysis are reported in Table 2 and N_2 sorption isotherms of MoO_x/PANI, MoS_x/PANI_thioA, and MoS_x/PANI_H_2S are shown in Figure S2. The S_{BET} values for MoO_x/PANI and MoS_x/PANI range between 6 and 8 m^2/g, consistently with the macroscopic geometric dimension of the PANI nanowires. The shape of the three isotherms corresponds to the type II, typical of non-porous or macroporous solids. Moreover, data suggest that, the sulfidation of MoO_x/PANI in liquid phase has no significant effect on the texture whereas the high temperature sulfidation by the removal of carbonaceous species decreases the amount of adsorbed N_2 and BET surface area as a consequence. The C, H, N, S contents in the samples were almost constant between MoO_x/PANI and MoS_x/PANI_thioA, whereas a sharp decrease in C, N and H contents was observed for MoS_x/PANI_H_2S due to a degradation of PANI at 350°C. The Mo wt% obtained from XRF data subtracting the contribution of the alumina diluent are in the range of conventional bulk catalysts.

Table 2. Elemental and textural analysis of unpromoted samples.

Samples	**S_{BET} (m^2/g)**	**Elemental analysis wt %**				**XRF wt%**
		C	**H**	**N**	**S**	**Mo**
MoO_x/PANI	8	18.2	2.6	3.7	-	38.7

MoS_x/PANI_thioA	6	17.5	1.8	3.6	32.8	40.6
MoS_x/PANI_H_2S	3	4.2	< 1	0.3	33.8	59.2

In order to identify the structure of MoO_x/PANI and MoS_x/PANI, powder XRD analysis was carried out (Figure 3). The pattern of the MoO_x/PANI looks like an amorphous molybdenum oxide. The diffraction peak (d-spacing 1.32 nm) is shifted at lower 2θ value indicative of the intercalation of PANI into the amorphous MoO_x layers as reported in literature [38] The diffraction pattern for MoS_x/PANI_thioA synthesized at 80°C exhibits a broad peak at 14° attributed to the formation of amorphous MoS_x. The crystallinity of the molybdenum sulfide is improved upon gas-phase sulfidation at 350°C and the diffraction peak of MoS_x/PANI_H_2S matches with hexagonal MoS_2 (ICDD: 04-008-2232; 2θ = 14°, 33.5° and 58.8° correspond to the respective (002), (100) and (110) lattice planes of MoS_2).

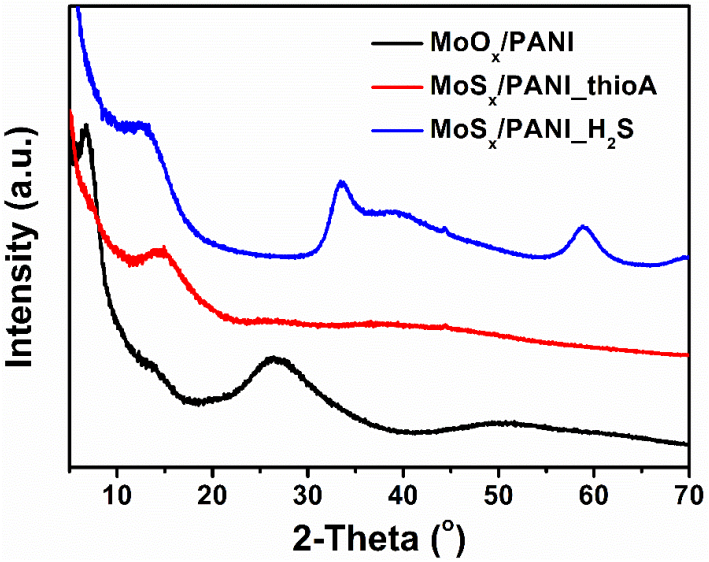

Figure 3. Powder XRD pattern of MoO_x/PANI, MoS_x/PANI_thioA, and MoS_x/PANI _H_2S.

Further, Raman spectroscopy was carried out in order to complete the description of the nature of molybdenum sulfide with respect to the sulfidation conditions. Raman spectra is shown on Figure 4. MoO_x/PANI sample exhibits bands corresponding to molybdenum oxide around 813, 875 and 960 cm^{-1} [41] and PANI main characteristic bands at 1172 (C-H bending), 1260 (C-N stretching), 1346 (C-$N^{+\cdot}$ stretching), 1495 (C=N stretching), 1564 (C-C stretching) and 1591 cm^{-1} (C=C stretching) [42]. After reflux sulfidation with thioacetamide at 80°C (MoS_x/PANI_thioA), the Raman bands correspond to PANI are preserved and a new set of

broad peaks appears at 160 and 220-230 cm^{-1} (corresponding to the Mo-S in-plane bending modes), 310-390 and 450 cm^{-1} (for the Mo-S stretching modes), and 520-555 cm^{-1} (S-S stretching modes). This could be attributed to the formation of MoS_3 and was further matched with standard MoS_3 [43,44]. On the other hand, MoS_x/PANI_H_2S obtained after gas-phase sulfidation at 350°C, has two Raman active bands located at 383 (E_{2g}) and 405 cm^{-1} (A_{1g}), which can be attributed to the crystalline MoS_2 phase [43]. Moreover, Raman bands for PANI were not observed anymore due to thermal decomposition at high temperature in agreement with CHNS results. Assuming the missing material from the CHNS analysis comes from residual oxygen combined to Mo to form MoO_3, and removing this contribution for the calculation of S/Mo ratio, 1.9 and 2.9 values corresponding to MoS_2 and MoS_3 are found respectively for MoS_x/PANI_H_2S and MoS_x/PANI_thioA in good agreement with Raman and XRD results. Roughly, 15% of Mo is still oxidized in MoS_x/PANI_thioA (resp. 8% for MoS_x/PANI_H_2S). MoO_x/PANI and MoS_x/PANI samples were further characterized by FTIR spectroscopy (Figure S4). The spectral band assignments corresponding to the molybdates, molybdenum sulfides and PANI are discussed After reflux sulfidation at 80ºC, the relative intensity of the peak observed at 975 cm^{-1} peak corresponding to the molybdate species decreased, while the absorption bands corresponding to PANI remained almost similar to the parent MoO_x/PANI. On the other hand, the absorption bands corresponding to PANI and molybdate species completely vanished after gas phase sulfidation at 350ºC, due to the degradation of PANI and high sulfidation degree of molybdates at 350ºC.

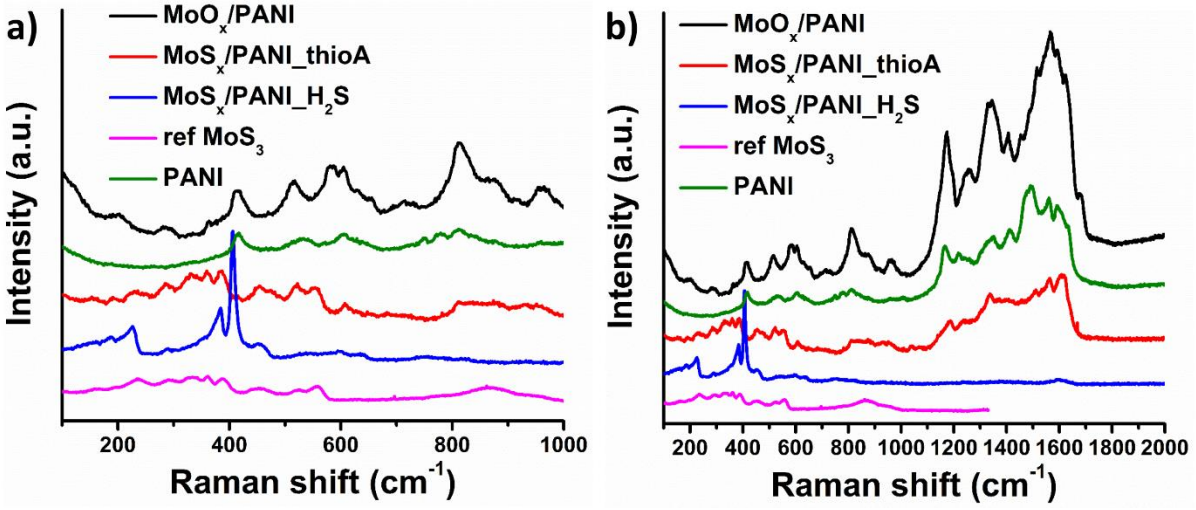

Figure 4. Raman spectra of reference MoS_3, reference PANI, MoO_x/PANI, MoS_x/PANI_thioA, and MoS_x/PANI_H_2S, plotted in the range of a) 100-1000 cm^{-1} and b) 100-2000 cm^{-1} Raman shift.

Finally, TGA analysis has been performed to assess the stability of the MoO_x/PANI and MoS_x/PANI_thioA samples (Figure S3 in supporting information). For both samples, the cumulative weight loss until 350°C is similar and close to 12%. This result confirms the good stability of the structures during the catalytic experiments as observed on the spent catalysts by microscopy. This allows us to discard a deep decomposition of the solid in the operating conditions of the catalytic test.

3.2 Characterization of promoted catalysts

MoO_x/PANI, MoS_x/PANI_thioA and MoS_x/PANI_H_2S samples were used as parent solids for the promotion step with cobalt acetylacetonate under different conditions. Bezverkhyy *et. al*. have shown that using cobalt acetylacetonate in organic solvents led to more active CoMoS phases than $Co(NO_3)_2.6H_2O$ due to the incorporation of cobalt into sulfided Mo after treatment with cobalt acetylacetonate [39] as shown by EXAFS. Over the years, other groups have established the importance of these promotion methods for alumina and carbon supported MoS_2 catalysts [45]. Table 3 summarizes the elemental analysis after the promotion step. Interestingly, the Co/Mo molar ratios are very close and correspond to the targeted values. Total metal amount (Mo+Co) in the range of 40-50 wt % are typical of conventional bulk catalysts and well above those of supported counterparts. We can also notice that $CoMoO_x$/PANI_65 contains less Co in agreement with the synthesis protocol including a washing step for the removal of unreacted Co precursors.

Generally speaking, no significant change in the CHNS contents with respect to the parent samples were noticed after the promotion step. Additionally, no visible change of the mesoscale morphologies was observed after $Co(acac)_2$ deposition as shown on SEM images (see Figure S5 for the $CoMoO_x$/PANI_65 as an example). as well as for the BET surface areas not reported here but not significantly modified. Similarly, no structural changes after promotion by Co were observed on powder XRD patterns (see Figure S6).

Table 3. XRF and CHNS elemental analysis of the promoted samples (before catalytic test).

Samples	**Elemental analysis wt%**				**XRF wt%**		**Co:Mo**	**S:Mo**
	C	**H**	**N**	**S**	**Mo**	**Co**	**mol/mol**	**mol/mol**
$CoMoO_x$/PANI_30	17.8	2.4	3.7	-	31.9	8.1	0.4	-
$CoMoS_x$/PANI_thioA_30	17.0	1.8	3.8	34.6	31.0	7.2	0.4	3.3
$CoMoS_x$/PANI_H_2S_30	5.7	< 1	0.6	36.6	40.3	8.7	0.4	2.7
$CoMoO_x$/PANI_65	24.8	2.8	4.5	-	31.9	5.6	0.3	-

Ref CoMoS	22.9	3.4	-	17.5	36.8	8.7	0.4	1.4

3.3 Catalyst characterization after catalytic tests

For convenient reasons, the labelling containing "MoO_x" was kept even if the spent catalysts are under their sulfided state and characterized by XPS and TEM as such.

- *X-Ray photoelectron spectroscopy (XPS)*

The decomposition of the S 2p, Mo 3d and Co 2p XPS spectra were performed using the corresponding oxide and sulfided references as supported monometallic catalysts and the decomposition methodology of $CoMo/Al_2O_3$ spectra set up by Gandubert *et al*. [46] The relative compositions are tabulated in Table 4. The Mo concentration of the PANI catalysts are quite similar (≈ 4 wt%) and lower than the reference due to a fraction of embedded Mo in the PANI matrix. Three different oxidation states of Mo, i.e. Mo^{+4}, Mo^{+5} and Mo^{+6} are detected which could be assigned to the MoS_2, molybdenum oxysulfide (MoO_xS_y) and molybdenum oxide (MoO_x) phases respectively (Figure 5a and Figures S7-9 in Sup Inf). XPS analysis shows that the main contribution corresponds to the desired phase Mo^{IV} (MoS_2) around 74-77% for the samples sulfided in liquid phase and higher (85%) for the $CoMoS_x$/PANI_H_2S_30 sulfided in gas phase, close to the ref CoMoS (89%) also sulfided in gas phase. The gas phase sulfidation thus allows a higher reduction of Mo^{V} (oxysulfide MoO_xS_y) into Mo^{IV} (MoS_2).

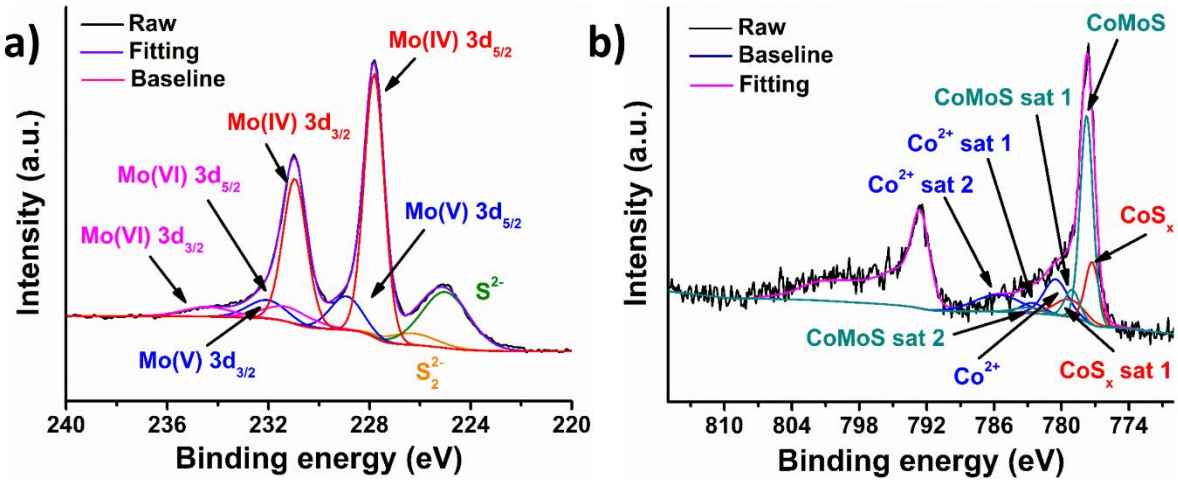

Figure 5: Spectral decompositions of high resolution a) Mo 3d and b) Co 2p ($2p_{3/2}$ region of the spectrum) core level spectrum of $CoMoO_x$/PANI_65 chosen as an example (spent sulfided catalyst).

Concerning the Co analysis, all the catalysts contain almost the same amount of Co at the surface except the $CoMoO_x$/PANI_65 (1.1% instead of 2-3 %) due to the removal of excess Co during the washing step. The highest content is observed for $CoMoS_x$/PANI_thioA_30. This tendency is in agreement with XRF results presented in Table 3. Co^{+2} (CoO), cobalt sulfide noted "CoS_x" but mainly under Co_9S_8 and catalytically active CoMoS phase were observed (Figure 5b). Among all the promoted catalysts, $CoMoO_x$/PANI_65 contains the highest fraction of Co as CoMoS phase (51%) with a low content of inactive CoS_x (20.1%) thus showing the beneficial effect of the removal of unreacted Co precursors on the formation of promoted mixed sites. Unreacted $Co(acac)_2$ is prone to form unreactive CoS_x during the gas phase sulfidation step. On the other hand, $CoMoS_x$/PANI_H_2S_30 exhibits a low CoMoS (14%) phase content associated with a low $(Co/Mo)_{slab}$ ratio. In our experiments, it can be stated that the nature of the unpromoted starting solid (i.e. oxidic amorphous sulfide as MoS_3 or crystallized as MoS_2) and synthesis conditions (i.e. washing step), affect the fraction of Co under CoMoS phase according the following sequence: MoO_x ($CoMoO_x$/PANI_65 > $CoMoO_x$/PANI_30) > MoS_3 ($CoMoS_x$/PANI_thioA_30) > MoS_2 ($CoMoS_x$/PANI_H_2S_30). This result is supported by the fact that the formation of mixed phases is favored when the sulfiding process occurs simultaneously for both metals Mo and Co [47], which qualitatively follows the same order. Cobalt acetylacetonate addition in the synthesis conditions as described in this paper is therefore less effective on a sulfided Mo phase than oxidic Mo phase likely due to weaker interactions with surface sites.

The binding energy values of Mo after deconvolution for all the promoted catalysts are given in Table S1. Among all these promoted catalysts, no major shift in $Mo3d_{5/2}$ peak positions was observed (+/- 0.3 experimental error). Interestingly, it was observed that surface Mo (wt%) concentrations measured by XPS are lower for PANI catalysts than the global Mo (wt%) concentrations obtained from XRF analysis. On the other hand, trends for Co (wt%) concentrations are found to be opposite i.e., higher surface Co concentrations are observed with respect to the global Co concentration. Since cobalt precursors are added after the polymerization process, the cobalt atoms remain mainly localized at the surface of the nanowires without encapsulation by carbon as in the case of a fraction of Mo.

Table 4. XPS analysis results of the spent (sulfided) catalysts.

Catalysts	At. Ratio Co/Mo slab*	% wt Mo	%wt Co	Mo species (% relative)			Co species (% relative)		
				MoS_2	MoO_xS_y	Mo^{+6}	CoMoS	CoS_x	Co^{+2}
$CoMoO_x$/PANI_30	0.25	3.8	2.1	75.9	11.3	12.8	21.1	37.2	41.7

$CoMoS_x$/PANI_thioA_30	0.30	3.9	2.9	77.7	11.6	10.8	19.1	30.0	50.9
$CoMoS_x$/PANI_H_2S_30	0.17	4.0	2.5	85.3	3.7	11.0	14.2	31.9	53.9
$CoMoO_x$/PANI_65	0.28	4.2	1.1	74.3	14.0	11.7	51.0	20.1	28.9
Ref CoMoS	0.11	7.7	2.3	89.3	1.4	9.3	21.3	31.4	47.4

* at ratio $\frac{Co}{Mo}(slab) = \frac{\%at\ Co * \%\ CoMoS}{\%at\ Mo * \%MoS_2}$

- *Transmission electron microscopy (TEM)*

TEM images of the different spent catalysts are presented on Figure 6. Length distributions of the slabs are shown on Figure 7 and values tabulated in Table 5.

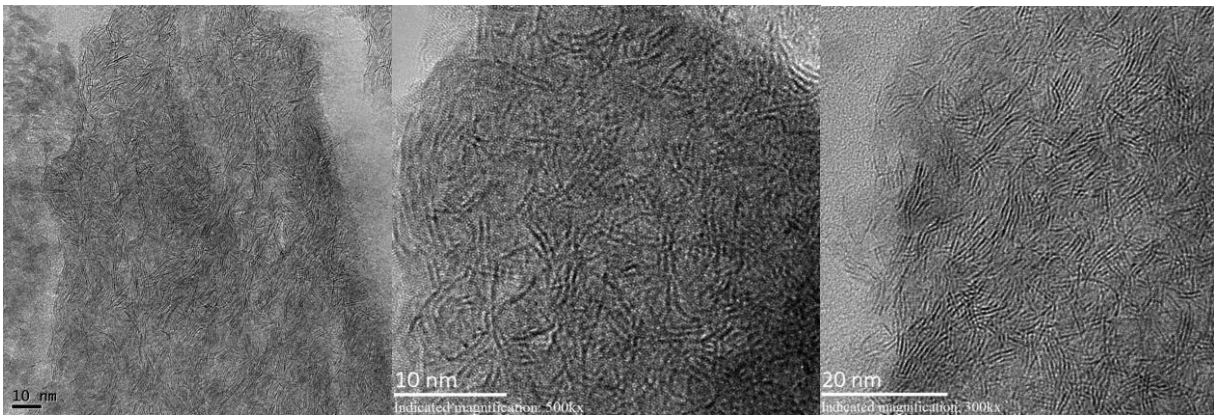

$CoMoO_x$/PANI_30 $CoMoO_x$/PANI_65 $CoMoS_x$/PANI_thioA_30

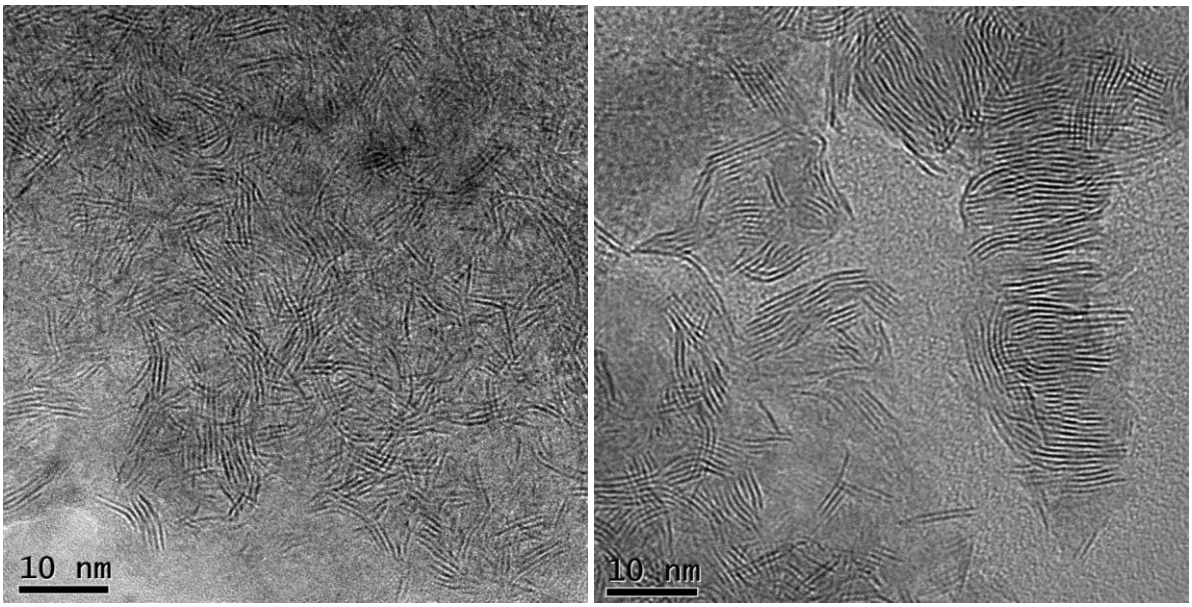

$CoMoS_x$/PANI_H_2S_30 Ref CoMoS

Figure 6: TEM images of the different spent catalysts.

All the PANI assisted synthesis led to a much lower mean size and stacking of MoS_2 slabs compared to the reference CoMoS catalyst prepared without PANI, thus showing its beneficial effect on the stabilisation against sintering, growth and aggregation. Among the PANI containing catalysts, $CoMoO_x$/PANI_65 exhibits the lowest average slab length and stacking values. This may be due to the different operating conditions during the Co addition (i.e. higher temperature) suggesting an influence of the temperature of Co impregnation on the final MoS_2 crystal size. We may hypothesize a partial dissolution and redispersion of MoO_x by some released acacH moieties coming from the reaction of $Co(acac)_2$ through a dissociative adsorption with the MoO_x surface by analogy with the results in ref [39].

Table 5 : Average slab lengths, fractions of $Mo_{edge+corner}$ (d_{TEM}), and average stacking values of the spent (sulfide) samples.

Catalysts	Average slab length (nm)	d_{TEM}= Mo $_{edges+corner}$ / Mo_{total} (%)*	Average stacking
$CoMoO_x$/PANI_30	5.1	22.0	2.8
$CoMoS_x$/PANI_thioA_30	4.3	25.5	2.6
$CoMoS_x$/PANI_H_2S_30	4.7	23.6	3.1
$CoMoO_x$/PANI_65	3.2	32.7	2.0
Ref CoMoS	7.4	15.7	4.3

* d_{TEM}: $\frac{\text{Mo } edges+corner}{Mo\ total} = \frac{\sum_i 6n_i - 6}{\sum_i 3n_i^2 - 3n_i + 1}$ with n_i : number of Mo atoms along one side of a MoS_2 slab determined from its length and i being the total number of slabs measured by TEM.

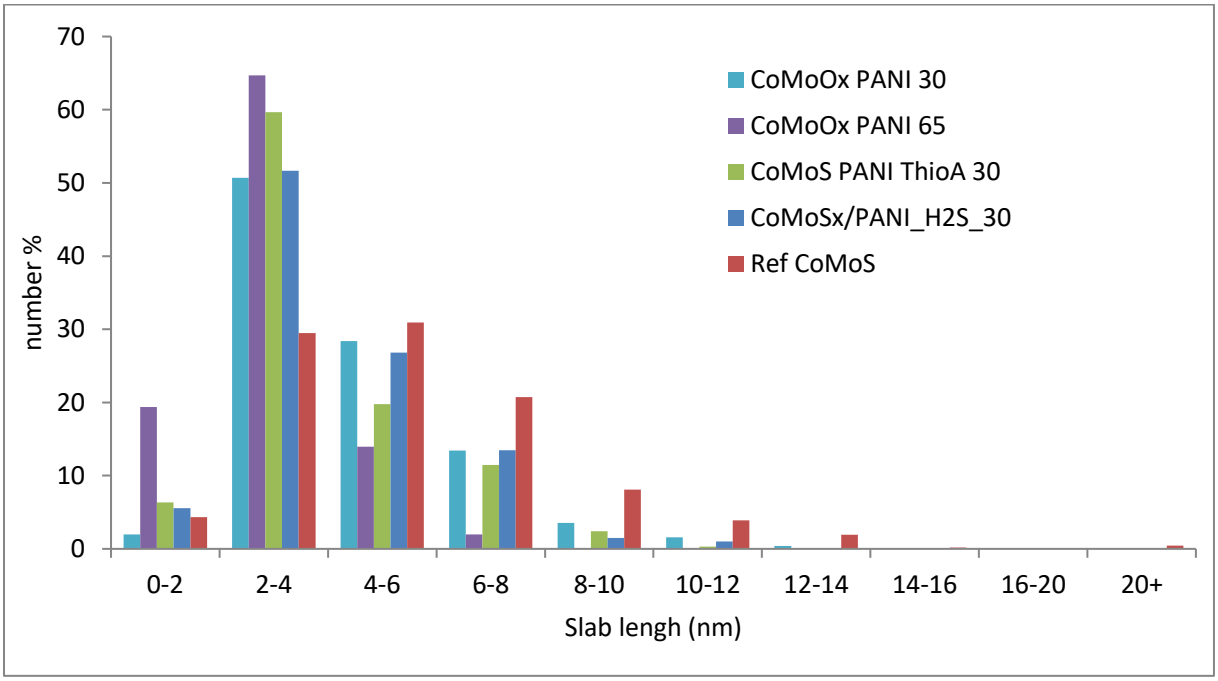

Figure 7: Slabs length distribution for the different spent catalysts.

3.4 Catalytic activity of promoted samples

Catalytic activities of promoted catalysts were evaluated under selective HDS conditions using 3-methylthiophene (3-MT) as reactant in presence of 2,3-dimethyl-2-butene (2,3-DM2BN). The first order rate constants for HDS of 3-MT and HYD of 2,3-DM2BN normalized by moles of MoS_2 from XPS and fraction of $Mo_{edges+corner}$ from MET are shown in d**)**

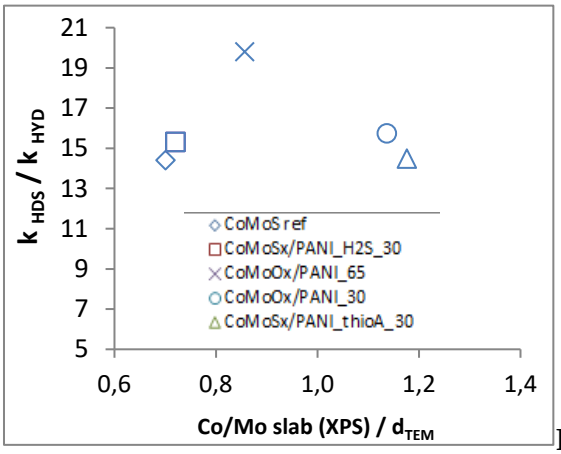

Figure 8. The apparent activation energies for HDS of 3-MT of all the promoted catalysts were around 22-35 kcal/mol, whereas for HYD of 2,3-DM2BN values in the range 20-32 kcal/mol were determined. From these data, it can be considered that the catalytic reactions fall in the chemical regime. The HDS and HYD rate constant of $CoMoS_x$/PANI_thioA_30 are the highest ones followed by those of $CoMoO_x$/PANI_30 whereas the two other catalysts gave performances very close to the reference CoMoS catalyst. Selectivity graph (selectivity factor k_{HDS}/k_{HYD} versus k_{HDS}) (Figure 8c) shows a classical behavior with an increase of HYD activity with HDS activity without large discrepancies between the catalysts, the highest selectivity being observed for $CoMoO_x$/PANI_65. Plotting the selectivity ratio versus the $(Co/Mo)_{edges+corner}$ atomic ratio defined as the ratio between $(Co/Mo)_{slab}$ and d_{TEM} ratio [1] seems to follow a maximum curve (Figure 8d). This result is in agreement with literature since it is usually reported that the promoter impacts much more HDS than HYD. As a consequence, the selectivity factor is supposed to follow the shape of the HDS curve versus the promoter content [2].

Plotting the normalized HDS rate constants (by mol of $(MoS_2)_{edges+corner}$) versus the $(Co/Mo)_{edges+corner}$ atomic ratio, a clear correlation for the different catalysts is observed (Figure

[1] $(Co/Mo)_{slab}$ / d_{TEM} ratio corresponds to the $(Co/Mo)_{edges+corner}$ atomic ratio calculated from the content in CoMoS phase (i.e.: at% Co*%$CoMoS_{XPS}$) divided by the amount of $Mo_{edges+corner}$ (at % Mo*%$MoS_{2\ XPS}$* d_{TEM})

9). Actually, the rate constant per mol $(MoS_2)_{edges+corner}$, which actually corresponds to a Turn Over Frequency (TOF), follows the $(Co/Mo)_{edges+corner}$ atomic ratio. Interestingly, this promotion effect is more pronounced on HDS when temperature increases (higher than 200°C) and for values higher than circa 0.9. This may be qualitatively supported by previous works on the influence of Co/Mo ratio and the ability to form active mixed sites by increasing the Co coverage of edges [48] as well as on the Mo-S bond strength and as a consequence on the catalytic activity [49,50].

Finally, HDS performances were assessed in a real gas-oil feedstock composed of straight-run gas oil (SRGO) and light cycle oil (LCO) containing 6815 ppm S. At 330°C, a total pressure of 40 bar and after 130 h of stabilization, $CoMo_x$/PANI_30 exhibited 95% of the activity expressed per mol Mo of an industrial Al_2O_3 supported CoMo catalyst and showed an 180% increase in the volumetric activity. This preliminary result is highly encouraging for the development of structured bulk hydrotreating catalysts.

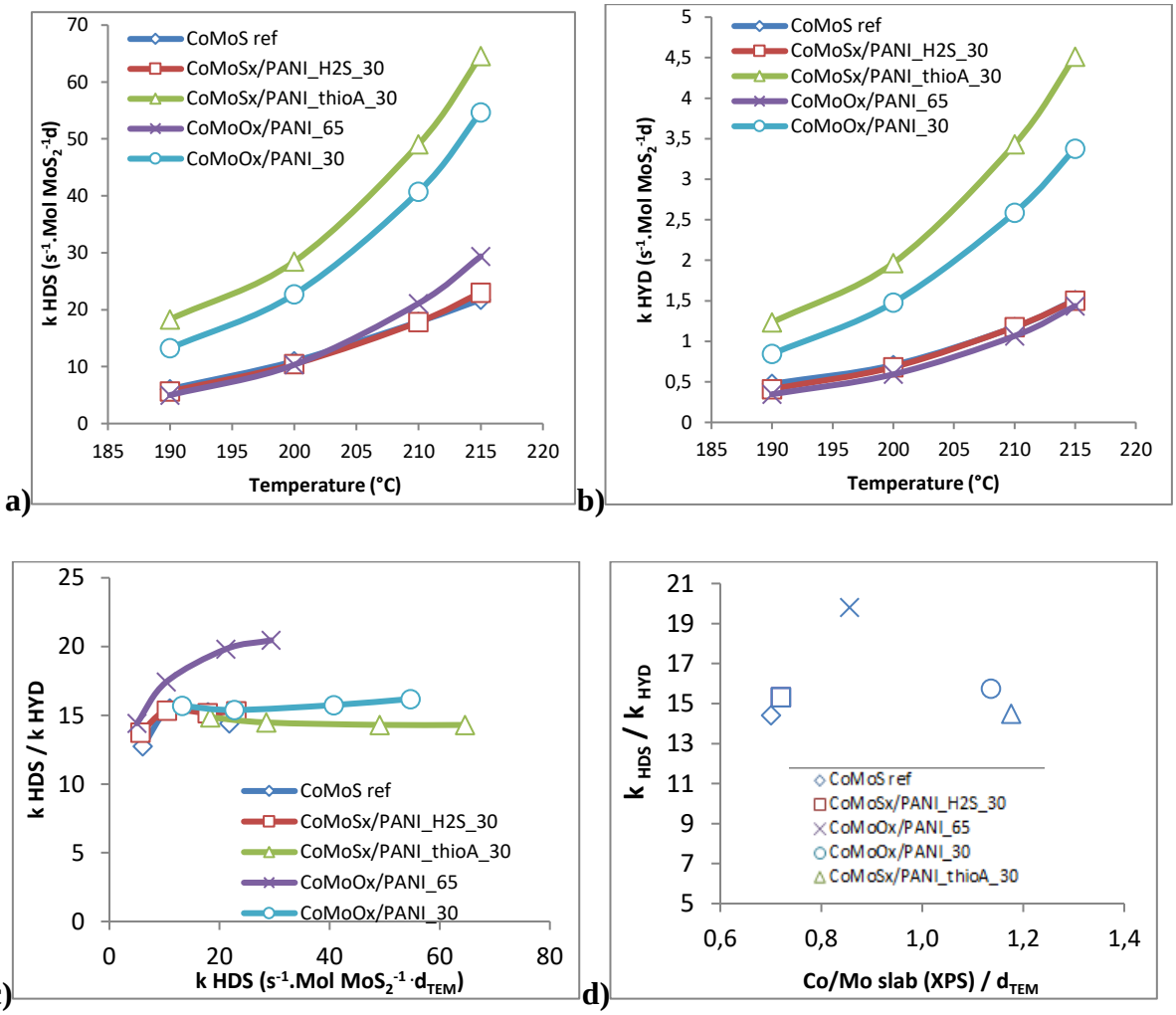

Figure 8: a) Normalized HDS rate constants (k_{HDS}) versus temperature, b) normalized HYD rate constants (k_{HYD}) versus temperature, c) k_{HDS}/k_{HYD} ratio versus k_{HDS} d) selectivity factor

(k_{HDS}/k_{HYD}) versus the $(Co/Mo)_{edges+corner}$ atomic ratio at a constant HDS conversion of ≈ 30% for the different catalysts.

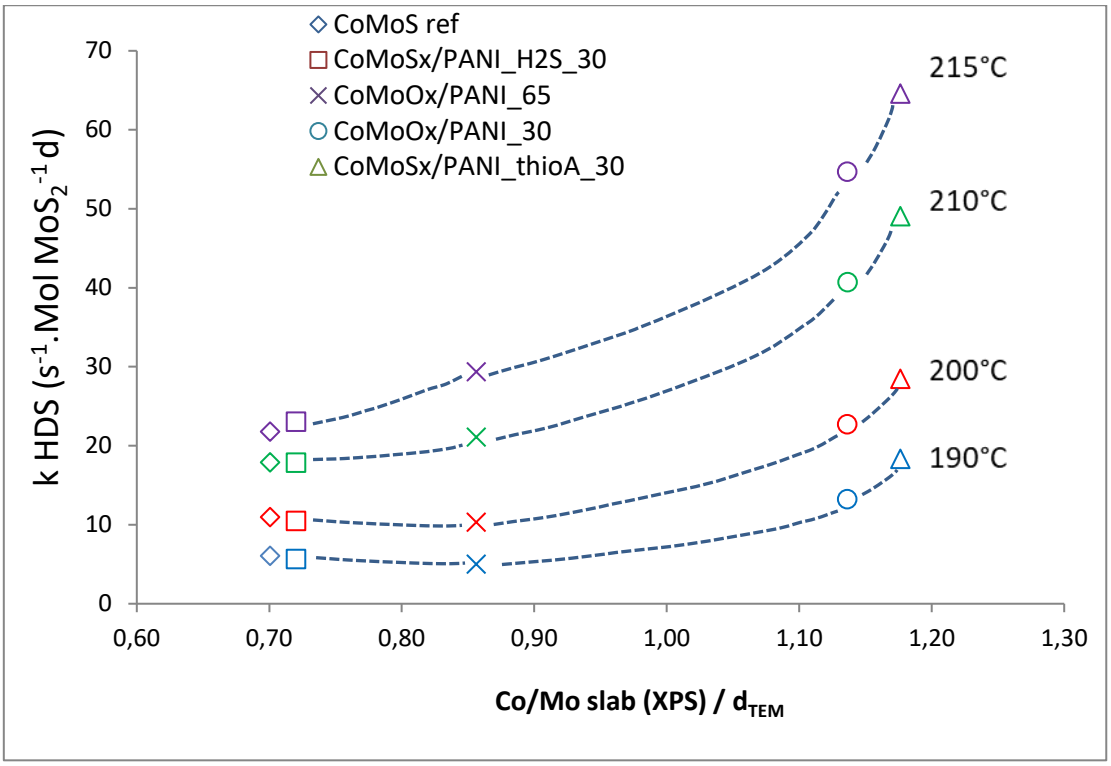

Figure 9: Normalized HDS rate constants k_{HDS} versus the $(Co/Mo)_{edges+corner}$ atomic ratio at different temperatures.

4. Conclusions

Catalytic performances of nanohybrid promoted CoMoS catalysts were greatly improved via a synthesis strategy based on the structuration of the active phase using self-assembled PANI nanowires. Promotion by a post-addition step of cobalt acetylacetonate via a surface reaction was performed on oxidic and sulfided Mo hybrids in different conditions. The results clearly show the beneficial effect of the PANI on the dispersion and stacking of CoMoS slabs and Co incorporation was found to be dependent on the type of Mo surface site.

Taking into account the different promotion levels, slabs lengths and stacking values determined by XPS and TEM, the highest rate constants normalized by mol of $(MoS_2)_{edges+corner}$ in the hydrodesulfurization of 3-methylthiophene were obtained with a sample of promoted CoMoS/PANI prepared from a MoS_3/PANI precursor. The normalized 3-methylthiophene HDS rate constants for all different samples have been correlated to the $(Co/Mo)_{edges+corner}$

atomic ratios (promotion factor) whereas an optimum versus the same ratio was observed for the HDS/HYD selectivity factor. In perspective of this work, the overall intrinsic catalytic activity of these bulk promoted catalysts could be further improved via an optimization of the nature of active sites (i.e. promotion level) or a gain in active phase accessibility playing with the dimensions, self-assembly properties or morphology of PANI structures.

5. Acknowledgments

The authors thank the Agence Nationale de la Recherche (ANR) for research project grant (ANR PASSCATA - ANR-16-CE07-0029). Authors also thank Virgile Rouchon, Veronique Lefebvre (IFPEN) and Julie Rousseau (IC2MP) for their assistance with the TEM data recording, Saloua Sahal-El-Ahrache, Christele Legens and Laurent Lemaitre (IFPEN) for XPS analysis.

1. A. Stanislaus, A. Marafi, M.S. Rana, Catal. Today 153 (2010) 1-68.
2. S. Brunet, D. Mey, G. Pérot, C. Bouchy, F. Diehl, Appl. Catal. A 278 (2005) 143-172.
3. H. Toulhoat, P Raybaud, Catalysis by transition metal sulphides. From molecular theory to industrial applications, Technip Editions, Paris, 2013.
4. A. Tanimu, K. Alhooshani, Energy & Fuels 33 (2019) 2810-2838.
5. J.N.D. de León, R.K. Chowdari, J. Antúnez-García, S. Fuentes-Moyado, Catalysts 9 (2019) 87.
6. R. Munirathinam, D. Laurenti, D. Uzio, G.D. Pirngruber, Appl. Catal. A 544 (2017) 116-125.
7. R. Munirathinam, D. Laurenti, G.D. Pirngruber, D. Uzio, ChemistrySelect 2 (2017) 2373-2382
8. D. Nicosia, R. Prins, J. Catal. 229 (2005) 424-438.
9. F. Rashidi, T. Sasaki, A.M. Rashidi, A.N. Kharat, K.J. Jozani, J. Catal. 299 (2013) 32-335.
10. S. Yao, Y. Zheng, L. Ding, S. Ng, H. Yang, Catal. Sci. Technol. 2 (2012) 1925–1932.
11. F. Trejo, M.S. Rana, J. Ancheyta, Catal. Today 130 (2008) 327-336.
12. J. Ramirez, S. Fuentes, G. Díaz, M. Vrinat, M. Breysse, M. Lacroix, Appl. Catal. 52 (1989) 211-223.
13. D. Gao, A. Duan, X. Zhang, Z. Zhao, E. Hong, J. Li, H. Wang, Appl. Catal. B 165 (2015) 269-284.
14. E. Furimsky, Ind. Eng. Chem. Res. 56 (2017) 11359-11371.
15. P.A. Nikulshin, D.I. Ishutenko, A.A. Mozhaev, K.I. Maslakov, A.A. Pimerzin, J. Catal. 312 (2014) 152-169.
16. M.A. Lélias, P.J. Kooyman, L. Mariey, L. Oliviero, A. Travert, J. van Gestel, J.A.R. van Veen, F. Maugé, J. Catal. 267 (2009) 14-23.
17. M. Breysse, C. Geantet, P. Afanasiev, J. Blanchard, M. Vrinat, Catal. Today 130 (2008) 3-13.

18. J.-S. Choi, F. Maugé, C. Pichon, J. Olivier-Fourcade, J.-C. Jumas, C. Petit-Clair, D. Uzio, Appl. Catal. A 267 (2004) 203-216.
19. L. Van Haandel, G.M. Bremmer, E.J.M. Hensen, T. Weber, J. Catal. 351 (2017) 95-106.
20. S. Eijsbouts, S.W. Mayo, K. Fujita, Appl. Catal. A 322 (2007) 58-66.
21. S. Eijsbouts, F. Plantenga, B. Leliveld, Y. Inoue, K. Fujita, Am. Chem. Soc. Div. Fuel Chem. 48 (2003) 494-495.
22. P Afanasiev, C.R. Chimie 11 (2008) 159-182.
23. S. Wang, C. An, J. Yuan, Materials 3 (2010) 401-433.
24. C. Fontaine, Y. Romero, A. Daudin, E. Devers, C. Bouchy, S. Brunet, Appl. Catal. A 388 (2010) 188-195.
25. Y.E. Armenta, J.C. Reyes, F.P. Delgado, M.D. Valle, G. Alonso, S. Fuentes, R.R. Rivera, Appl. Catal. A 486 (2014) 62-68.
26. Z. Le, P. Afanasiev, D. Li, Y. Shi, M. Vrinat, C.R. Chimie 11 (2008) 130-136.
27. D. Genuit, I. Bezverkhyy, P. Afanasiev, J. Solid State Chem. 178 (2005) 2759-2765.
28. C. Zhang, P. Li, X. Liu, T. Liu, Z. Jiang, C. Li, Appl. Catal. A 556 (2018) 20-28.
29. P. Li, Y. Chen, C. Zhang, B. Huang, X. Liu, T. Liu, Z. Jiang, C. Li, Appl. Catal. A 533 (2017) 99-108.
30. A. Nogueira, R. Znaiguia, D. Uzio, P. Afanasiev, G. Berhault, Appl. Catal. A 429-430 (2012) 92-105.
31. P. Afanasiev, Appl. Catal. B 227 (2018) 44-53.
32. V. Hetier, D. Pena, A. Carvalho, L. Courthéoux, V. Flaud, E. Girard, D. Uzio, S. Brunet, P. Lacroix-Desmazes, A. Pradel, Catalysts 9 (2019), 793.
33. H. Liu, C. Yin, X. Li, Y. Chai, Y. Li, C. Liu, Catal. Today 282 (2017) 222-229.
34. C. Yin, L. Zhao, Z. Bai, H. Liu, Y. Liu, C. Liu, Fuel 107 (2013) 873-878.
35. A.N. Varakin, A.V. Mozhaev, A.A. Pimerzin, P.A. Nikulshin, Appl. Catal. B 238 (2018) 498-508.
36. N.A. Dhas, K.S. Suslick, J. Am. Chem. Soc. 127 (2005) 2368-2369.
37. G. Wang, G. Chen, W. Xie, W. Wang, L. Bing, Q. Zhang, H. Fu, F. Wang, D. Han, Fuel Processing Technology 199 (2020) 106268, https://doi.org/10.1016/j.fuproc.2019.106268.
38. L. Yang, S. Wang, J. Mao, J. Deng, Q. Gao, Y. Tang, O.G. Schmidt, Adv. Mater. 25 (2013) 1180-1184.
39. I. Bezverkhyy, P. Afanasiev, M. Lacroix, J. Catal. 230 (2005) 133-139.
40 S. Kasztelan, H. Toulhoat, J. Grimblot, J.P. Bonnelle, Appl. Catal. 13 (1984) 127.
41. M.A. Bañares, I.E. Wachs, J. Raman Spectrosc. 33 (2002) 359-380.
42. M. Trchová; Z. Morávková; M. Bláha; J. Stejskal, Electrochim. Acta 122 (2014) 28-38.
43. C.H. Chang; S.S. Chan, J. Catal. 72 (1981) 139-148.
44. Th. Weber, J.C. Muijsers, J.W. Niemantsverdriet, J. Phys. Chem. 99 (1995) 9194-9200.
45 D Laurenti, B Phung-Ngoc, Ch Roukoss, E Devers, K Marchand, L Massin, L Lemaitre, Ch Legens, AA Quoineaud, M Vrinat J. Catal. 297 (2013) 165-175.
46 A. Gandubert, C. Legens, D. Guillaume, S. Rebours, E. Payen, Oil Gas Sci. Technol.-Rev. IFP 62 (1) (2007).
47 P. Blanchard, N. Frizi, S. Mary, P. Baranek, Ch. Lancelot, C. Lamonier, E. Payen, C. R. Chimie 19 (2016) 1286-1302
48 E. Krebs, B.Silvi, P. Raybaud Catal. Today Vol 130, Issue 1, 2008, 160-169.
49 P. Raybaud, J. Hafner, G. Kresse, S. Kasztelan, H. Toulhoat, J. Catal. 190 (2000) 128.
50 A.D. Gandubert, E. Krebs, C. Legens, D. Costa, D. Guillaume, P. Raybaud Catalysis Today 130 (2008) 149-159.